HHS Public Access

Author manuscript

Neuroimage. Author manuscript; available in PMC 2021 August 04.

Published in final edited form as:

Neuroimage. 2021 February 01; 226: 117627. doi:10.1016/j.neuroimage.2020.117627.

Functional imaging of the brainstem during visually-guided motor control reveals visuomotor regions in the pons and midbrain

Winston T. Chu[a,b], **Trina Mitchell**[b], **Kelly D. Foote**[c,d], **Stephen A. Coombes**[b], **David E. Vaillancourt**[a,b,d,*]

[a]J. Crayton Pruitt Family Department of Biomedical Engineering, University of Florida, P.O. Box 116131, Gainesville, FL 32611-6131, USA

[b]Department of Applied Physiology and Kinesiology, University of Florida, P.O. Box 118205, Gainesville, FL 32611-8205, USA

[c]Department of Neurosurgery, University of Florida, Gainesville, FL 32611, USA

[d]Norman Fixel Institute for Neurological Diseases, University of Florida, 3009 SW Williston Rd, Gainesville, FL 32608, USA

Abstract

Integrating visual information for motor output is an essential process of visually-guided motor control. The brainstem is known to be a major center involved in the integration of sensory information for motor output, however, limitations of functional imaging in humans have impaired our knowledge about the individual roles of sub-nuclei within the brainstem. Thus, the bulk of our knowledge surrounding the function of the brainstem is based on anatomical and behavioral studies in non-human primates, cats, and rodents, despite studies demonstrating differences in the organization of visuomotor processing between mammals. fMRI studies in humans have examined activity related to visually-guided motor tasks, however, few have done so while controlling for both force without visual feedback activity and visual stimuli without force activity. Of the studies that have controlled for both conditions, none have reported brainstem activity. Here, we employed a novel fMRI paradigm focused on the brainstem and cerebellum to systematically investigate the hypothesis that the pons and midbrain are critical for the integration of visual information for motor control. Visuomotor activity during visually-guided pinch-grip force was measured while

*Corresponding author at: Department of Applied Physiology and Kinesiology, University of Florida, P.O. Box 118205, Gainesville, FL 32611-8205, USA. vcourt@ufl.edu (D.E. Vaillancourt).

Credit authorship contribution statement

Winston T. Chu: Conceptualization, Data curation, Formal analysis, Investigation, Methodology, Project administration, Software, Supervision, Validation, Visualization, Writing - original draft, Writing - review & editing. **Trina Mitchell:** Conceptualization, Formal analysis, Investigation, Methodology, Project administration, Validation, Writing - review & editing. **Kelly D. Foote:** Methodology, Writing - review & editing. **Stephen A. Coombes:** Conceptualization, Methodology, Project administration, Supervision, Validation, Writing - review & editing. **David E. Vaillancourt:** Conceptualization, Data curation, Funding acquisition, Methodology, Project administration, Resources, Supervision, Validation, Writing - original draft, Writing - review & editing.

Declaration of Competing Interest

None.

Supplementary materials

Supplementary material associated with this article can be found, in the online version, at doi:10.1016/j.neuroimage.2020.117627.

controlling for force without visual feedback activity and visual stimuli without force activity in healthy adults. Using physiological noise correction and multiple task repetitions, we demonstrated that visuomotor activity occurs in the inferior portion of the basilar pons and the midbrain. These findings provide direct evidence in humans that the pons and midbrain support the integration of visual information for motor control. We also determined the effect of physiological noise and task repetitions on the visuomotor signal that will be useful in future studies of neurodegenerative diseases affecting the brainstem.

Keywords

Brainstem; Visually-guided; Motor control; fMRI

1. Introduction

Vision is the most relied upon sensory input for directing movement in humans. Studies in non-human primates and cats have shown that visual information of object location projects from the inferior parietal lobe to the pontine nuclei in the brainstem, and from the pontine nuclei through mossy fibers to the cerebellum (Albus et al., 1981; Mishkin et al., 1983; Glickstein, 2000). However, differences between mammals in cortical visual area projections to pontine nuclei and midbrain connectivity have been demonstrated and thus it is unknown how much of this knowledge translates to visuomotor processing in humans (Brodal, 1972; Glickstein et al., 1985; Aravamuthan et al., 2009; Alam et al., 2011). Although animal studies provide an essential foundation for our understanding of the visuomotor system, functional neuroimaging studies in humans with appropriate control conditions are necessary to fully understand how visual information is integrated for motor control in humans.

Many functional neuroimaging studies have investigated the visuomotor system in humans. However, few have done so while appropriately controlling for other processes that occur during visually-guided motor control. Both force without visual feedback activity and visual stimulus without force activity must be controlled for to isolate activity related to the integration of visual information for motor control. Furthermore, the force produced during the visually-guided motor task should match the force produced during the motor task without visual feedback because force amplitude is directly related to functional magnetic resonance imaging (fMRI) blood-oxygen level dependent (BOLD) signal amplitude (Dai et al., 2001; Spraker et al., 2007, 2012). The visual stimuli should also be identical to the feedback given in the visually-guided motor task since saccadic processing has been demonstrated in the brainstem and cerebellum (Ellermann et al., 1998; Miall et al., 2000).

Inherent properties of fMRI limit the quality of the signal in the brainstem (Brooks et al., 2013; Beissner, 2015). Brainstem visuomotor activity in humans is rarely detected in functional imaging studies despite almost all reporting extensive activation of the cerebellum (Ellermann et al., 1998; Jueptner, 1998; Miall et al., 2000; Vaillancourt et al., 2003; Nitschke et al., 2005; Kuhtz-Buschbeck et al., 2008; Keisker et al., 2010). Furthermore, to our knowledge visuomotor activity in the brainstem has never been detected while controlling

for both force without visual feedback activity and visual stimuli without force activity. The brainstem signal is susceptible to motion artifacts and physiological noise due to its proximity to surrounding CSF, the pulsatile motion of the basilar artery, and the natural elongation during respiration (Klose et al., 2000; Harvey et al., 2008; Chang et al., 2009; Beissner et al., 2011). In the current study, RETROICOR (Glover et al., 2000) was used to reduce the effects of physiological noise from respiration and heart rate. Inspired by electroencephalography literature (Kappenman and Luck, 2010), signal averaging was also explored as a technique to enhance the visuomotor brainstem signal. We analyzed the effectiveness of these approaches to improve signal quality and determine the most effective procedures for detecting brainstem functional activity in humans.

In the current study, we tested the hypothesis that, in humans, the pons and midbrain are directly involved in visuomotor processing. Three variations of a visually-guided motor task were used to detect visuomotor activity while controlling for activity related to the visual stimulus alone and the production of force alone. Functional imaging of the brainstem and cerebellum required the development and implementation of a scan protocol and processing pipeline optimized for this region of the brain. To better understand the factors that enable the detection of the brainstem fMRI signal, activity maps were computed with and without correction for physiological noise. Additionally, subsets of the total number of task repetitions were analyzed independently to determine the effect of these repetitions on the brainstem signal.

2. Materials and methods

2.1. Participants

Data was collected on 20 healthy right-handed individuals (Male:Female = 9:11; age range = 19–26 years). The subjects all had corrected or normal vision and none of the subjects had any history of neurological disorder. All participants gave written informed consent and all procedures were approved by the local Institutional Review Board. The work described has been carried out in accordance with The Code of Ethics of the World Medical Association (Declaration of Helsinki) for experiments involving humans. Anonymized data and code are available from the corresponding author upon reasonable request.

2.2. Experimental design

Fig. 1 illustrates the key aspects of the experimental design. Participants laid supine in the MRI scanner and performed a pinch-grip task using their right thumb to press an MRI-compatible force transducer. Force applied to the force transducer bends an embedded fiber-optic cable that was connected to an SM130 Optical Sensing Interrogator (Micron Optics). The force was then digitized at 125 Hz and converted to Newtons using a custom program built in LabVIEW (National Instruments). The fiber-optic force transducer was subsequently able to achieve a resolution of 0.025 N. Visual feedback according to the task condition was provided to the participant inside the scanner through a screen visible from within the scanner using a mirror. The screen showed two horizontal bars and was otherwise black to minimize visual stimuli unrelated to the task.

Participants performed 3 different tasks in a 30-s block paradigm (alternating between rest and task). The three tasks (Fig. 1B) were force-vision, force-only, and vision-only. In the force-vision task, two horizontal bars were visible to the participant. The bottom bar moved linearly to indicate the force produced and the static top bar indicated the target force. The goal of the task was to press on the force transducer such that the bottom bar overlapped with the top bar. The bottom bar turned green to indicate when the participant should press and turned red to indicate when they should stop pressing. The target force was set to 15% of each participant's maximum voluntary contraction (MVC). During the 30 s force-vision task block, participants alternated between 2 s of applying the target force and 1 s of rest for 10 iterations.

In the force-only task, participants were instructed to apply force at 15% of MVC but to do so without visual feedback. The color of the visual feedback bar switched from red to green to indicate when the participant should press on the force transducer, however, the bar did not move when the force transducer was pressed. During the 30 s force-only task block, participants alternated between 2 s of applying force and 1 s of rest for 10 iterations, as in the force-vision condition.

In the vision-only task, participants were instructed to not apply any force during the duration of the 30 s task block. During the vision-only task, the subjects were shown a recording of the visual feedback they received in a previous trial of the force-vision task. Each fMRI scan consisted of four 30 s task blocks of each of the three tasks (force-vision, force-only, vision-only). Each 30 s task block was preceded and proceeded by a 30 s rest block and the task fMRI scan was repeated three times. Before the start of the scan, all participants were trained on the three tasks and were allowed to practice all task conditions two times.

2.3. Maximum voluntary contraction calculation and force data processing

The participant's MVC for the task was calculated before the scan. Participants were instructed to produce their maximum force for 5 s for 3 trials. The MVC was taken as the average sustained force across the three trials and used in the subsequent experiments in the scanner. Force metrics during the experiment were calculated for each participant from the middle 1 s of each 2 s pulse to capture the error in the sustained force portion of the pulse. The average force amplitude produced and root-mean-square error (RMSE) were calculated separately for the force-vision and the force-only tasks.

2.4. fMRI acquisition

MRI images were collected on a 3T Siemens Magnetom Prisma. The scanner was equipped with a 64-channel head/neck phased array coil with 48 channels in the head region and 16 channels in the neck region. Functional MRI scans were collected using an EPI sequence: repetition time = 2500 ms, echo time = 30 ms, flip angle = 80°, echo spacing = 0.64 ms, field of view = 240 × 240 mm, voxel size = 2.5 mm isotropic, no gap between slices, transverse interleaved slices = 40, measurements = 300, and a GRAPPA imaging scheme was employed with an acceleration factor of 2 in the phase encoding direction. The field of view was positioned inferior to the corpus callosum and superior to the inferior edge of the

medulla oblongata. Whole-brain T1-weighted images were collected to improve image registration (repetition time = 2000 ms; echo time = 2.99 ms; inversion time = 1010 ms; flip angle = 8°; field of view = 256 mm; voxel size = 0.8 mm isotropic, no gap between slices, transverse interleaved slices = 208). For the duration of the fMRI scans, pulse and respiration rate data were recorded using a pulse oximeter placed on the middle finger of the left hand and a respiration belt placed on the torso. Small cushions were placed around the participant's head to restrict head motion.

2.5. fMRI data analysis

Task fMRI data were processed using a combination of custom shell scripts, the AFNI toolbox (https://afni.nimh.nih.gov), and the SUIT Matlab toolbox (http://www.diedrichsenlab.org/imaging/suit.htm). fMRI data were preprocessed using the afni_proc.py script from the AFNI toolbox. The first 3 vol. of each fMRI scan were removed to allow for the stabilization of the T1 signal. The scans were despiked and the effects of pulse and respiration on the fMRI signal were removed using the RETROICOR method (Glover et al., 2000). The pulse and respiration timeseries data were converted into slice-based regressors using the RetroTS.m script from the AFNI toolbox for regressing out components of heart rate, respiration, and respiration volume per time from the fMRI signal. Slices within each volume were time-shifted to that of the first slice and each volume was spatially registered to the last volume for motion correction. 6 motion parameters (roll, pitch, yaw, and their first derivatives) were saved from the spatial registration step for use as regressors of no interest during the regression analysis. If the head motion between adjacent volumes exceeded 0.5 mm, both volumes were excluded from the regression analysis. The average head motion between adjacent volumes was 0.09 ± 0.03 mm and the average number of volumes removed was 5.0 ± 10.6 vol. (300 vol. per scan). The EPI image was linearly registered to the subject's T1 image and each voxel's timeseries was scaled to have a mean of 100 and range of 0 to 200. The general linear model analysis was then performed. The BOLD signal during the task periods was modeled by boxcar regressors convolved with a finite impulse response function ($h(t)=t^4e^{-t}/[4^4e^{-4}]$) for each task (Friston et al., 1995; Cox, 1996; Cohen, 1997). Beta-coefficient maps for each task condition from the general linear model represent the amplitude of BOLD activation for that task.

Beta-coefficient maps in subject-space were registered into SUIT template space (Diedrichsen, 2006; Diedrichsen et al., 2009) using the SPM 8 and SUIT Matlab toolboxes. The subject-space T1 anatomical images were aligned to the SPM 8 white-matter template. The cerebellum and brainstem were then isolated and nonlinearly registered to the SUIT template (Ashburner and Friston, 1999). The calculated transformations were applied to the beta-coefficient maps in subject-space to warp them into SUIT template space (nearest-neighbor interpolation). The SUIT template is at 1 mm isotropic resolution and thus the registered beta-coefficient maps are also at 1 mm isotropic resolution. Beta-coefficient maps in template space were then smoothed with a 2 mm full-width half-maximum Gaussian kernel to reduce the effects of registration errors. The smoothed beta-coefficient maps in template space represent the amplitude of BOLD activation for each task and were used in the group-level statistical analysis.

Group-level t-statistic maps were generated for the three task conditions and were thresholded at $p<0.001$. We corrected for multiple comparisons by using the -Clustsim option in AFNI's 3dttest++. This yielded a family-wise error corrected p-value of 0.05 which was achieved as a voxel-level p-value threshold of 0.001 and a cluster threshold of 73 mm^3 (Cox, 1996). The cluster threshold was calculated by simulating noise-only random volumes based on the input datasets. Importantly, this cluster threshold method controls for the false positive rate without assuming a shape for the spatial autocorrelation function. Contrast maps were created on the difference between force-vision and force-only in addition to the difference between force-vision and vision-only. The force-vision vs. force-only difference map statistically tests for regions of force-vision activity not associated with the production of force. The force-vision vs. vision-only difference map statistically tests for regions of force-vision activity not associated with the processing of the visual stimuli. Regions of the brainstem and cerebellum common to both difference maps and the force-vision map represent areas involved in the integration of visual information with motor output for visually-guided motor control (visuomotor activity).

Characterization of the visuomotor activity clusters in the midbrain was difficult given the size of brainstem nuclei and the lack of overt landmarks visible in a T1 scan. To locate the region of the cuneiform nucleus, an MNI space atlas was used to identify surrounding prominent regions on slice $z=-6$ including the red nucleus, substantia nigra, subthalamic nucleus, and cerebral peduncle (Lucerna, 2002). Consultation of additional atlases and a DBS neurosurgeon (co-author K. D. F.) led us to label the region of the cuneiform nucleus (Naidich and Duvernoy, 2009; Mai and Paxinos, 2012) within slice $z=-6$. To locate the region of the pedunculopontine nucleus, a procedure specific to identifying the pedunculopontine nucleus was used (Zrinzo et al., 2008). This procedure is outlined in Supplementary Fig. 1. Surrounding landmark regions from figures in Zrinzo et al., 2008 were outlined to aid in identifying the region of the pedunculopontine nucleus. Identification of the region of the pedunculopontine nucleus was confirmed by a functional neurosurgeon/neuroanatomist (co-author K. D. F.).

Anatomical evidence has shown that the descending cortico-ponto-cerebellar and cortico-olivo-cerebellar pathways descend from the cortex to the ipsilateral brainstem and then cross to the contralateral cerebellum (Glickstein et al., 1994; Kandel et al., 2000; Palesi et al., 2017). To test the hypothesis that the force-vision activity is higher in the contralateral brainstem compared to the ipsilateral brainstem (relative to the task), an ROI approach was employed. A mask of the left (contralateral) brainstem activity was created and mirrored to the right (ipsilateral) side to create left and right brainstem ROIs in template space. The average activity (beta-coefficient) within these regions was calculated for each subject. This analysis was repeated in the cerebellum to determine if the force-vision activity is greater in the ipsilateral cerebellum compared to the contralateral cerebellum. The left and right force-vision activity masks for the brainstem and cerebellum are shown in Supplementary Fig. 2.

2.6. Protocol development analyses

Primary hypotheses were tested using all data across the three scan repetitions, corresponding to 12 task block repetitions (four task block repetitions per scan) for each task

condition. This amount of data (360 s per task condition) was collected in anticipation of poor signal quality in the brainstem and the majority of task-fMRI studies do not collect such a large amount of data per task condition. To determine the minimum amount of data necessary for robust detection of visuomotor brainstem activity we used a signal averaging approach in the statistical ANOVA. Here, signal averaging is defined as averaging the beta-coefficients within the context of the ANOVA as a repeated factor. All statistical analyses were repeated using either one (120 s per task condition), two (240 s per task condition), or three scan (360 s per task condition) repetitions from each subject. The total volume of activity within the brainstem and cerebellum was then calculated for each analysis condition.

To determine the effect of physiological correction on the detected brainstem activity during visuomotor processing, the fMRI analysis was repeated (using all 3 scan repetitions) without including physiological regressors in the regression analysis. A force-vision activity map without correction for physiological signals was subsequently created for comparison to the force-vision activity map with physiological correction. The average signal to noise ratio (SNR) and peak signal to noise ratio (PSNR) were calculated on each subject's force-vision beta-coefficient map, with and without physiological correction.

2.7. Statistical analyses

Statistical analyses were performed using AFNI tools and SPSS. Comparisons of the force produced between force-vision and force-only task conditions were assessed with 2 × 3 ANOVAs (2: force-vision and force-only, 3: scan repetition). Voxel-wise ANOVAs (3 levels: scan 1, scan 2, and scan 3) were used to create the force-vision, force-only, and vision-only maps as well as the contrast maps (force-vision vs. force-only and force-vision vs. vision-only). Left and right force-vision activity were compared using 2 × 3 ANOVAs (2: left and right; 3: scan repetition). For the scan repetition analysis, a voxel-wise one-way ANOVA (2 levels: scan 1 and scan 2) and voxel-wise one-sample *t*-test were used to create the force-vision maps that only included data from 2 scans and 1 scan respectively. For all statistical maps, a *p*-value threshold of 0.001 was applied and a cluster threshold of 73 mm^3 was used. The method used to calculate the threshold is described above. Statistical comparison of the effect of physiological correction on the SNR and PSNR was performed using two 2 × 3 ANOVAs (2: with and without physiological correction; 3: scan repetition).

3. Results

3.1. Force production in young healthy adults

Participants had an MVC of 71.75 ± 11.42 N (mean ± SD) and were tasked with producing a force of 15% of their MVC. During the force-vision task, the mean force of each pulse was 14.51 ± 0.41% MVC with a root-mean-square error of 0.76 ± 0.35 N for a duration of 2.03 ± 0.10 s. During the force-only task, participants produced a force of 14.58 ± 4.67% MVC with a root-mean-square error of 3.92 ± 1.52 N for a duration of 1.95 ± 0.13 s. No significant differences ($p>0.5$) in force produced or force produced relative to MVC was found between the force-vision and force-only task conditions.

3.2. Force-vision task induces activity in the brainstem and cerebellum

Fig. 2 (rows 1–3) shows the brainstem and cerebellum activation maps for the three task conditions. Table 1 gives the center of mass of significant clusters in MNI coordinates for each task condition. The brainstem activity related to the force-vision task was observed in the midbrain, pons, and medulla, with a prominent cluster in the caudal region of the basilar pons. This force-vision activity in the brainstem was bilateral, however, a significantly larger average BOLD signal was found in the left brainstem, contralateral to the force-producing hand ($p = 0.001$) (Fig. 3A). The force-vision task also induced broad and bilateral activation in the cerebellum, with a large area of activation centered at right lobule VI of the cerebellum. Comparison of left and right cerebellar activity in each subject showed a significantly larger force-vision BOLD signal in the right cerebellum, ipsilateral to the force-producing hand ($p<0.001$) (Fig. 3B). The force-only task induced activity in a smaller set of regions of the cerebellum compared to the force-vision task (Fig. 2, row 2 and Table 1). This activity was observed bilaterally but was largely centered on right lobule VI of the cerebellum. Force-only activity was not observed in the brainstem. The vision-only task did not induce any statistically significant activity in the brainstem or cerebellum.

3.3. Visuomotor activation observed in the pons and midbrain

To determine the regions activated in visuomotor processing, difference maps for force-vision compared to force-only and force-vision compared to vision-only were computed. The force-vision vs. force-only difference map demonstrated that force-vision produced a higher degree of activation in the midbrain, pons, and cerebellum compared to force-only (Fig. 2, row 4 and Fig. 3C). The force-vision vs. vision-only difference maps demonstrated that force-vision produced a higher degree of activation in the midbrain, pons, medulla, and cerebellum compared to vision-only (Fig. 2, row 5 and Fig. 3C). Regions commonly activated in force-vision, and the two difference maps are regions that are unique to visually-guided force production and likely involved in the integration of visual information for motor output. As shown in Fig. 3C, three regions (designated by green, blue, and pink circles) were observed to be commonly activated in force-vision and the two difference maps: right posterior basal pons (center of mass [x,y,z]: [4,−33,−43]), region of the left cuneiform nucleus (center of mass [x,y,z]: [−7,−28,−7]), and region of the right pedunculopontine nucleus (center of mass [x,y,z]: [6,−32,−17]) (Lucerna, 2002; Zrinzo et al., 2008; Naidich and Duvernoy, 2009; Mai and Paxinos, 2012). To better visualize regions common to the force-vision, force-vision vs. force-only difference map, and force-vision vs. vision-only difference map, a binary overlap map was created (Fig. 4A). The region of the cuneiform nucleus and region of the pedunculopontine nucleus were identified relative to surrounding regions traced from MNI-space atlases (Fig. 4B) (Lucerna, 2002; Zrinzo et al., 2008; Mai and Paxinos, 2012).

3.4. Detection of significant visuomotor activity in the brainstem was dependent on collecting a large number of task repetitions

To determine the minimum number of task repetitions necessary for robust detection of activity in the brainstem, subsets of the task-fMRI dataset were created using 4 and 8 task repetition blocks (30 s each) for comparison to the full dataset (12 task repetition blocks).

The force-vision activation maps were re-computed using the task repetition subsets (Fig. 5). Four repetitions of the 30 s task blocks (120 s of task duration) produced 1317 mm^3 of activity in the brainstem using our scan protocol and optimized processing procedure (Fig. 5B, row 1). A total of eight task block repetitions produced a 123% increase in detected activity (2939 mm^3) in the brainstem (Fig. 5B, row 2). When using 12 task block repetitions we observed a total of 5497 mm^3 of activity in the brainstem (317% increase compared to 4 task block repetitions) with a large cluster of activity in the posterior region of the basilar pons (Fig. 5B, row 3). The cerebellum followed a similar trend although the increases in activity volume were less pronounced. 120 s of task duration produced 24,344 mm^3 in the cerebellum and this increased by 59% and 102% for 240 s and 360 s of task duration, respectively.

3.5. Effects of retroicor correction for physiological noise on the visuomotor brainstem signal

Fig. 6 illustrates the effects of the physiological noise correction on the detected force-vision activity. SNR and PSNR were calculated for each subject's force-vision beta-coefficient map. An ANOVA was run and the estimated marginal means for the effect of physiological correction are given in Fig. 6A and B. No significant differences were found between corrected and uncorrected data in both SNR or PSNR metrics ($p > 0.05$). Group-wise force-vision activity maps reveal subtle differences between the corrected and uncorrected maps (Fig. 6C).

4. Discussion

In this study, a novel fMRI paradigm was developed to systematically investigate visuomotor activity in the brainstem and cerebellum. Using physiological noise correction, a template specialized for the brainstem and cerebellum, and a large number of task repetitions, visuomotor activity was detected reliably for the first time in the pons and midbrain while controlling for force-only and vision-only activity. Furthermore, our results corroborate prior studies detecting visuomotor activity in the cerebellum. An investigation into the effects of task repetitions revealed that doubling and tripling the amount of data collected per subject increased the group-level volume of significant activity in the brainstem by 123% and 317%, respectively, whereas the volume of activity in the cerebellum only increased by 59% and 102%, respectively. Correction for physiological noise was observed to not significantly change the SNR or PSNR of the force-vision beta-coefficient images. Overall, our results provide direct evidence in humans that the pons and midbrain are critical for integrating visual information for motor control. Our unique protocol and task paradigm illustrates the importance of task repetitions, particularly in the brainstem, and may prove useful in future studies of neurodegenerative diseases affecting the brainstem.

Pontine projections are a major brainstem target of efferent fibers from the visual and motor cortical regions (Glickstein, 2000). Studies in non-human primates, cats, and excised human brain tissue have revealed robust structural connections from the motor (Leichnetz et al., 1984; Schmahmann and Pandya, 1997) and visual (Albus et al., 1981; Glickstein et al.,

1994) cortical regions to pontine nuclei and from pontine nuclei to the cerebellum (Tomasch, 1969). Functional evidence of the role of cortical and cerebellar regions in visually-guided motor control has been demonstrated through neural recordings in non-human primates (Mushiake et al., 1991; Mushiake and Strick, 1993), PET imaging studies in humans (Jueptner, 1998), and fMRI studies in humans (Ellermann et al., 1998; Miall et al., 2000; Vaillancourt et al., 2003; Nitschke et al., 2005; Kuhtz-Buschbeck et al., 2008; Keisker et al., 2010), though the role of the pons is not well known. By controlling for both force-only and vision-only activity, our findings provide direct evidence in humans that the pons is critical for the integration of visual information for motor control. Furthermore, our results corroborate the previously well-established role of the cerebellum in visuomotor control.

Force-vision activity was observed throughout the midbrain, however, only the pedunculopontine nucleus and cuneiform nucleus areas were differentially activated in force-vision compared to force-only and vision-only activity. These regions make up the mesencephalic reticular formation which has been most commonly associated with locomotion in animals (Shik et al., 1966; Mori et al., 1978; Takakusaki et al., 2003). Recently, these regions have been explored as potential targets for deep brain stimulation to alleviate gait disturbances in Parkinson's disease patients (Mestre et al., 2016; Chang et al., 2020). Furthermore, it is also thought that these two regions are involved in the integration of sensory information for motor output (Ryczko and Dubuc, 2013). Optogenetic stimulation in the mesencephalic locomotor region in mice has been shown to increase the gain of visual responses even at stimulation levels that do not evoke overt movement (Lee et al., 2014). Although together the cuneiform nucleus and pedunculopontine nucleus form the mesencephalic locomotor region, evidence suggests that each of these regions has unique connectivity and function.

The cuneiform nucleus is located caudal and lateral to the superior colliculus and medial to the lateral lemniscus. The cuneiform nucleus has connections to and from many regions related to sensory input and motor output such as the superior colliculus, hypothalamus, periaqueductal gray, zona incerta, preoptic area, and lateral geniculate nucleus (Edwards and de Olmos, 1976; Zemlan and Behbehani, 1988; Gatto and Goulding, 2018). Although associated with gait, the function of the cuneiform nucleus is complex and, in fact, is not essential to gait as illustrated by a lesion study in rats that showed that excitotoxic lesions of the cuneiform nucleus had no significant effect on spontaneous or accumbens-stimulated locomotion (Allen et al., 1996). Stimulation studies in rodents have shown that the cuneiform nucleus is associated with the integration of sensory information for motor control in the context of aversive behaviors (Mitchell et al., 1988; Depoortere et al., 1990; Gatto and Goulding, 2018) and nociceptive reflexes (Zemlan and Behbehani, 1988). Our results in combination with these findings preliminarily suggest that the cuneiform nucleus area integrates visual information for movements beyond aversive locomotion behaviors to include upper limb motor control in humans. Additional functional imaging studies are needed in humans to establish the mechanisms behind this observation.

The pedunculopontine nucleus is located in the dorsolateral portion of the ponto-mesencephalic tegmentum and, compared to the cuneiform nucleus, has a more diverse set of connected regions including the motor cortex, basal ganglia, thalamus, brainstem,

cerebellum, and spinal cord (French and Muthusamy, 2018). There is abundant evidence relating the pedunculopontine nucleus to the modulation of locomotion, with recent work identifying the unique roles of glutamatergic and cholinergic pedunculopontine nucleus neurons in mice (Caggiano et al., 2018). Anatomical and functional evidence exists that suggests that the pedunculopontine nucleus plays a role in the integration of visual information for motor control. The pedunculopontine nucleus receives inputs from multiple regions involved in visual processing including the superior colliculus, lateral geniculate nucleus, and the pulvinar. Furthermore, it has been shown in a cohort of Parkinson's disease patients that stimulation of the pedunculopontine nucleus influences visual contrast sensitivity (Strumpf et al., 2016). There is also evidence suggesting that the role of the pedunculopontine nucleus could extend beyond lower limb motor control required for locomotion to include upper limb motor control. In a diffusion MRI study, it was shown that connections between the pedunculopontine nucleus and upper extremity portion of the motor cortex were detected in 87.5% of patients while connections to lower extremity and trunk regions of the motor cortex were detected in 62.5% and 56.25% of patients, respectively (Muthusamy et al., 2007). Furthermore, in a study involving Parkinson's disease patients that had received deep brain stimulation electrodes placed in the pedunculopontine nucleus, it was shown that significant pre-movement potentials were observed preceding wrist movements (Tsang et al., 2010). Our observation that the pedunculopontine nucleus region is involved in the integration of visual information for motor control aligns with these findings and suggests that the role of the pedunculopontine nucleus region may extend beyond sensory integration for locomotion to include upper limb motor control.

The topography of force-vision activity in the brainstem and cerebellum aligns with known anatomical patterns of laterality and the role of the cerebellum. Although force-vision activity was observed bilaterally in the brainstem, the activity was significantly higher in the left brainstem, which was contralateral to the hand producing force. In the cerebellum, bilateral force-vision activity was also observed, however, the right cerebellum had increased activity, which is ipsilateral to the hand producing force. It is well known that the contralateral motor cortex is activated in unilateral movement. The downstream cortico-ponto-cerebellar, cortico-olivo-cerebellar, and upstream cerebello-thalamo-cortical pathways connect the cortex to the cerebellum and are integral to vision and motor control. These pathways have been shown to pass from the cortex through the ipsilateral brainstem and cross to the contralateral cerebellum (Glickstein et al., 1994; Kandel et al., 2000; Palesi et al., 2017).

While other functional imaging studies in humans have examined activity during visually-guided movement, activity in the brainstem is rarely detected. Previous fMRI studies on visually-guided motor control typically collect a total duration of data (epoch duration x epoch repetitions x subjects) within the range of 422–3200 s for a single task condition (Ellermann et al., 1998; Miall et al., 2000; Vaillancourt et al., 2003; Kuhtz-Buschbeck et al., 2008; Keisker et al., 2010; Holmström et al., 2011; Mayhew et al., 2017). In this study, we demonstrate that a relatively large number of task repetitions (twelve 30 s force-vision task blocks in 20 subjects = 7200 s) was necessary to detect large clusters of force-vision activity in the brainstem. It should be noted that even with more than three times more data collected than a typical fMRI study, we do not appear to have reached a plateau in force-vision signal

improvement. Thus, it is possible that if more data were collected the force-vision signal would improve further. We also demonstrate that the effect of signal averaging is not consistent throughout the brain and is more pronounced in the brainstem compared to the cerebellum. This is expected, given that physiological noise in the brainstem is high relative to the rest of the brain (Beissner et al., 2011; Brooks et al., 2013) and thus there is more room for improvement by signal averaging. A limitation of this analysis is that we are unable to obtain a ground-truth of the force-vision activity and thus must interpret the results under the base assumption that averaging the signal from a larger sample of data increases the likelihood that the average is closer to the true signal.

RETROICOR accounts for the effects of physiological noise by deconvoluting pulse and respiration signals collected during the scan from the fMRI signal (Glover et al., 2000). In this study, we did not find a significant difference between with and without physiological correction in the SNR or PSNR of the force-vision beta-coefficient maps. A slight reduction in activation volume is visible in the group-wise force-vision activity map with physiological correction compared to without physiological correction. Previous analyses on the RETROICOR technique have shown improvements in temporal SNR, however, the authors warn that RETROICOR may reduce task activity signals if the physiological noise and the task-related activity are correlated (Glover et al., 2000). It should be noted that RETROICOR is not the only technique for using physiological signals to reduce noise in fMRI signals; other techniques such as RETROKCOR (Hu et al., 1995) and DRIFTER (Särkkä et al., 2012) may produce more stark improvements in data quality.

5. Conclusions

In this study, we provide the first detailed functional imaging evidence of pontine and mesencephalic involvement in visuomotor control in humans by applying appropriate control conditions and a specialized imaging protocol. We show that the posterior region of the basal pons and the mesencephalic reticular formation are specifically involved in the integration of visual information for upper limb motor output. Furthermore, we determined the effects of signal averaging and physiological correction on the brainstem visuomotor signal. We demonstrated that signal averaging improved the visuomotor activity signal and had a disproportionately large effect on the brainstem signal. The results from this study provide a much-needed window into the complex functions of the human brainstem. Our analyses into the factors that affected the detection of brainstem activity can inform future fMRI studies aiming to explore pathological or therapeutic modulators of brainstem activity.

Supplementary Material

Refer to Web version on PubMed Central for supplementary material.

Acknowledgments

This work was supported by NIH grants R01 NS058487 and T32 NS082128.

Data and code availability statement

Anonymized data and code are available from the corresponding author upon reasonable request.

Abbreviations:

fMRI	functional magnetic resonance imaging
BOLD	blood oxygen level dependent
MVC	maximum voluntary contraction
RMSE	root-meansquare error
SNR	average signal to noise ratio
PSNR	peak signal to noise ratio

References

Alam M, Schwabe K, Krauss JK, 2011. The pedunculopontine nucleus area: critical evaluation of interspecies differences relevant for its use as a target for deep brain stimulation. Brain 134, 11–23. [PubMed: 21147837]

Albus K, Donate-Oliver F, Sanides D, Fries W, 1981. The distribution of pontine projection cells in visual and association cortex of the cat: an experimental study with horseradish peroxidase. J. Comp. Neurol 201, 175–189. [PubMed: 7287925]

Allen LF, Inglis WL, Winn P, 1996. Is the cuneiform nucleus a critical component of the mesencephalic locomotor region? An examination of the effects of excitotoxic lesions of the cuneiform nucleus on spontaneous and nucleus accumbens induced locomotion. Brain Res. Bull 41, 201–210. [PubMed: 8924029]

Aravamuthan BR, McNab JA, Miller KL, Rushworth M, Jenkinson N, Stein JF, Aziz TZ, 2009. Cortical and subcortical connections within the pedunculopontine nucleus of the primate Macaca mulatta determined using probabilistic diffusion tractography. J. Clin. Neurosci 16, 413–420. [PubMed: 19167229]

Ashburner J, Friston KJ, 1999. Nonlinear spatial normalization using basis functions. Hum. Brain Mapp 7, 254–266. [PubMed: 10408769]

Beissner F, 2015. Functional MRI of the brainstem: common problems and their solutions. Clin. Neuroradiol 25, 251–257. [PubMed: 25981409]

Beissner F, Deichmann R, Baudrexel S, 2011. fMRI of the brainstem using dual-echo EPI. Neuroimage 55, 1593–1599, [PubMed: 21256220]

Brodal P, 1972. The corticopontine projection from the visual cortex in the cat. II. The projection from areas 18 and 19. Brain Res 39, 319–335. [PubMed: 4113020]

Brooks JCW, Faull OK, Pattinson KTS, Jenkinson M, 2013. Physiological noise in brainstem fMRI. Front. Hum. Neurosci 7. Available at 10.3389/fnhum.2013.00623/abstract. Accessed January 10, 2020. [PubMed: 23372547]

Caggiano V, Leiras R, Goñi-Erro H, Masini D, Bellardita C, Bouvier J, Caldeira V, Fisone G, Kiehn O, 2018. Midbrain circuits that set locomotor speed and gait selection. Nature 553, 455–460. [PubMed: 29342142]

Chang C, Cunningham JP, Glover GH, 2009. Influence of heart rate on the BOLD signal: the cardiac response function. Neuroimage 44, 857–869, [PubMed: 18951982]

Chang SJ, Cajigas I, Opris I, Guest JD, Noga BR, 2020. Dissecting brainstem locomotor circuits: converging evidence for cuneiform nucleus stimulation. Front. Syst. Neurosci 14, 64. [PubMed: 32973468]

Cohen MS, 1997. Parametric analysis of fMRI data using linear systems methods. Neuroimage 6, 93–103. [PubMed: 9299383]

Cox RW, 1996. AFNI: software for analysis and visualization of functional magnetic resonance neuroimages. Comput. Biomed. Res 29, 162–173. [PubMed: 8812068]

Dai T, Liu J, Sahgal V, Brown R, Yue G, 2001. Relationship between muscle output and functional MRI-measured brain activation. Exp. Brain Res 140, 290–300. [PubMed: 11681304]

Depoortere R, Sandner G, Di Scala G, 1990. Aversion induced by electrical stimulation of the mesencephalic locomotor region in the intact and freely moving rat. Physiol. Behav 47, 561–567. [PubMed: 2359770]

Diedrichsen J, 2006. A spatially unbiased atlas template of the human cerebellum. Neuroimage 33, 127–138. [PubMed: 16904911]

Diedrichsen J, Balsters JH, Flavell J, Cussans E, Ramnani N, 2009. A probabilistic MR atlas of the human cerebellum. Neuroimage 46, 39–46, [PubMed: 19457380]

Edwards SB, de Olmos JS, 1976. Autoradiographic studies of the projections of the midbrain reticular formation: ascending projections of nucleus cuneiformis. J. Comp. Neurol 165, 417–431. [PubMed: 1262539]

Ellermann JM, Siegal JD, Strupp JP, Ebner TJ, Ugurbil K, 1998. Activation of visuomotor systems during visually guided movements: a functional MRI study. J. Magn. Reson 131, 272–285. [PubMed: 9571103]

French IT, Muthusamy KA, 2018. A review of the pedunculopontine nucleus in Parkinson's disease. Front. Aging Neurosci 10. Available at 10.3389/fnagi.2018.00099/full. Accessed September 11, 2020. [PubMed: 29441011]

Friston KJ, Holmes AP, Poline J-B, Grasby PJ, Williams SCR, Frackowiak RSJ, Turner R, 1995. Analysis of fMRI time-series revisited. Neuroimage 2, 45–53. [PubMed: 9343589]

Gatto G, Goulding M, 2018. Locomotion control: brainstem circuits satisfy the need for speed. Curr. Biol 28, R256–R259. [PubMed: 29558639]

Glickstein M, 2000. How are visual areas of the brain connected to motor areas for the sensory guidance of movement? Trends Neurosci 23, 613–617. [PubMed: 11137151]

Glickstein M, Gerrits N, Kralj-Hans I, Mercier B, Stein J, Voogd J, 1994. Visual pontocerebellar projections in the macaque. J. Comp. Neurol 349, 51–72, [PubMed: 7852626]

Glickstein M, May JG, Mercier BE, 1985. Corticopontine projection in the macaque: the distribution of labelled cortical cells after large injections of horseradish peroxidase in the pontine nuclei. J. Comp. Neurol 235, 343–359. [PubMed: 3998215]

Glover GH, Li T-Q, Ress D, 2000. Image-based method for retrospective correction of physiological motion effects in fMRI: RETROICOR. Magn. Reson. Med 44, 162–167, [PubMed: 10893535]

Harvey AK, Pattinson KTS, Brooks JCW, Mayhew SD, Jenkinson M, Wise RG, 2008. Brainstem functional magnetic resonance imaging: disentangling signal from physiological noise. J. Magn. Reson. Imaging 28, 1337–1344. [PubMed: 19025940]

Holmström L, de Manzano Ö, Vollmer B, Forsman L, Valero-Cuevas FJ, Ullén F, Forssberg H, 2011. Dissociation of brain areas associated with force production and stabilization during manipulation of unstable objects. Exp. Brain Res 215, 359–367. [PubMed: 22038714]

Hu X, Le TH, Parrish T, Erhard P, 1995. Retrospective estimation and correction of physiological fluctuation in functional MRI. Magn. Reson. Med 34, 201–212, [PubMed: 7476079]

Jueptner M, 1998. A review of differences between basal ganglia and cerebellar control of movements as revealed by functional imaging studies. Brain 121, 1437–1449. [PubMed: 9712006]

Kandel ER, Schwartz JH, Jessell TM, 2000. Principles of Neural Science, 4th ed. McGraw-Hill, Health Professions Division, New York.

Kappenman ES, Luck SJ, 2010. The effects of electrode impedance on data quality and statistical significance in ERP recordings. Psychophysiology doi:10.1111/j.1469-8986.2010.01009.x, Accessed May 18, 2020.

Keisker B, Hepp-Reymond M-C, Blickenstorfer A, Kollias SS, 2010. Differential representation of dynamic and static power grip force in the sensorimotor network. Eur. J. Neurosci 31, 1483–1491. [PubMed: 20384781]

Klose U, Strik C, Kiefer C, Grodd W, 2000. Detection of a relation between respiration and CSF pulsation with an echoplanar technique. J. Magn. Reson. Imaging 11, 438–444. [PubMed: 10767073]

Kuhtz-Buschbeck JP, Gilster R, Wolff S, Ulmer S, Siebner H, Jansen O, 2008. Brain activity is similar during precision and power gripping with light force: an fMRI study. Neuroimage 40, 1469–1481. [PubMed: 18316207]

Lee AM, Hoy JL, Bonci A, Wilbrecht L, Stryker MP, Niell CM, 2014. Identification of a brainstem circuit regulating visual cortical state in parallel with locomotion. Neuron 83, 455–466. [PubMed: 25033185]

Leichnetz GR, Smith DJ, Spencer RF, 1984. Cortical projections to the paramedian tegmental and basilar pons in the monkey. J. Comp. Neurol 228, 388–408. [PubMed: 6480918]

Lucerna S, 2002. In Vivo Atlas of Deep Brain Structures: With 3D Reconstructions Springer, Berlin.

Mai JK, Paxinos G, 2012. The Human Nervous System, 3rd ed. Elsevier Academic Press, Amsterdam ; Boston.

Mayhew SD, Porcaro C, Tecchio F, Bagshaw AP, 2017. fMRI characterisation of widespread brain networks relevant for behavioural variability in fine hand motor control with and without visual feedback. Neuroimage 148, 330–342. [PubMed: 28093359]

Mestre TA, Sidiropoulos C, Hamani C, Poon Y-Y, Lozano AM, Lang AE, Moro E, 2016. Long-term double-blinded unilateral pedunculopontine area stimulation in Parkinson's disease: a 4-year blinded assessment of PPN stimulation for PD. Mov. Disord 31, 1570–1574. [PubMed: 27392513]

Miall RC, Imamizu H, Miyauchi S, 2000. Activation of the cerebellum in co-ordinated eye and hand tracking movements: an fMRI study. Exp. Brain Res 135, 22–33. [PubMed: 11104124]

Mishkin M, Ungerleider LG, Macko KA, 1983. Object vision and spatial vision: two cortical pathways. Trends Neurosci 6, 414–417.

Mitchell IJ, Dean P, Redgrave P, 1988. The projection from superior colliculus to cuneiform area in the rat: II. Defence-like responses to stimulation with glutamate in cuneiform nucleus and surrounding structures. Exp. Brain Res 72. Available at: 10.1007/BF00250607. Accessed September 9, 2020. [PubMed: 3416959]

Mori S, Nishimura H, Kurakami C, Yamamura T, Aoki M, 1978. Controlled locomotion in the mesencephalic cat: distribution of facilitatory and inhibitory regions within pontine tegmentum. J. Neurophysiol 41, 1580–1591. [PubMed: 731291]

Mushiake H, Inase M, Tanji J, 1991. Neuronal activity in the primate premotor, supplementary, and precentral motor cortex during visually guided and internally determined sequential movements. J. Neurophysiol 66, 705–718. [PubMed: 1753282]

Mushiake H, Strick PL, 1993. Preferential activity of dentate neurons during limb movements guided by vision. J. Neurophysiol 70, 2660–2664. [PubMed: 8120605]

Muthusamy KA, Aravamuthan BR, Kringelbach ML, Jenkinson N, Voets NL, Johansen-Berg H, Stein JF, Aziz TZ, 2007. Connectivity of the human pedunculopontine nucleus region and diffusion tensor imaging in surgical targeting. JNS 107, 814–820.

Naidich TP, Duvernoy HM, 2009. Duvernoy's Atlas of the Human Brain Stem and Cerebellum: High-Field MRI: Surface Anatomy, Internal Structure, Vascularization and 3D Sectional Anatomy Springer, WienNew York.

Nitschke MF, Arp T, Stavrou G, Erdmann C, Heide W, 2005. The cerebellum in the cerebro-cerebellar network for the control of eye and hand movements — an fMRI study. In: Progress in Brain Research Elsevier, pp. 151–164 Available at:.

Palesi F, De Rinaldis A, Castellazzi G, Calamante F, Muhlert N, Chard D, Tournier JD, Magenes G, D'Angelo E, Gandini Wheeler-Kingshott CAM, 2017. Contralateral cortico-ponto-cerebellar pathways reconstruction in humans in vivo: implications for reciprocal cerebro-cerebellar structural connectivity in motor and non-motor areas. Sci. Rep 7, 12841. [PubMed: 28993670]

Ryczko D, Dubuc R, 2013. The multifunctional mesencephalic locomotor region. Curr. Pharm. Des 19, 4448–4470. [PubMed: 23360276]

Särkkä S, Solin A, Nummenmaa A, Vehtari A, Auranen T, Vanni S, Lin F-H, 2012. Dynamic retrospective filtering of physiological noise in BOLD fMRI: DRIFTER. Neuroimage 60, 1517–1527. [PubMed: 22281675]

Schmahmann JD, Pandya DN, 1997. Anatomic organization of the basilar pontine projections from prefrontal cortices in rhesus monkey. J. Neurosci 17, 438–458. [PubMed: 8987769]

Shik ML, Severin FV, Orlovskĭ GN, 1966. Control of walking and running by means of electric stimulation of the midbrain. Biofizika 11, 659–666. [PubMed: 6000625]

Spraker MB, Corcos DM, Kurani AS, Prodoehl J, Swinnen SP, Vaillancourt DE, 2012. Specific cerebellar regions are related to force amplitude and rate of force development. Neuroimage 59, 1647–1656. [PubMed: 21963915]

Spraker MB, Yu H, Corcos DM, Vaillancourt DE, 2007. Role of individual basal ganglia nuclei in force amplitude generation. J. Neurophysiol 98, 821–834. [PubMed: 17567775]

Strumpf H, Noesselt T, Schoenfeld MA, Voges J, Panther P, Kaufmann J, Heinze H-J, Hopf J-M, 2016. Deep brain stimulation of the pedunculopontine tegmental nucleus (PPN) influences visual contrast sensitivity in human observers avenanti A, ed. PLoS ONE 11, e0155206. [PubMed: 27167979]

Takakusaki K, Habaguchi T, Ohtinata-Sugimoto J, Saitoh K, Sakamoto T, 2003. Basal ganglia efferents to the brainstem centers controlling postural muscle tone and locomotion: a new concept for understanding motor disorders in basal ganglia dysfunction. Neuroscience 119, 293–308, [PubMed: 12763089]

Tomasch J, 1969. The numerical capacity of the human cortico-pontocerebellar system. Brain Res 13, 476–484, [PubMed: 5305681]

Tsang EW, Hamani C, Moro E, Mazzella F, Poon YY, Lozano AM, Chen R, 2010. Involvement of the human pedunculopontine nucleus region in voluntary movements. Neurology 75, 950–959. [PubMed: 20702790]

Vaillancourt DE, Thulborn KR, Corcos DM, 2003. Neural Basis for the Processes That Underlie Visually Guided and Internally Guided Force Control in Humans. J. Neurophysiol 90, 3330–3340. [PubMed: 12840082]

Zemlan FP, Behbehani MM, 1988. Nucleus cuneiformis and pain modulation: anatomy and behavioral pharmacology. Brain Res 453, 89–102. [PubMed: 2456838]

Zrinzo L, Zrinzo LV, Tisch S, Limousin PD, Yousry TA, Afshar F, Hariz MI, 2008. Stereotactic localization of the human pedunculopontine nucleus: atlas-based coordinates and validation of a magnetic resonance imaging protocol for direct localization. Brain 131, 1588–1598. [PubMed: 18467343]

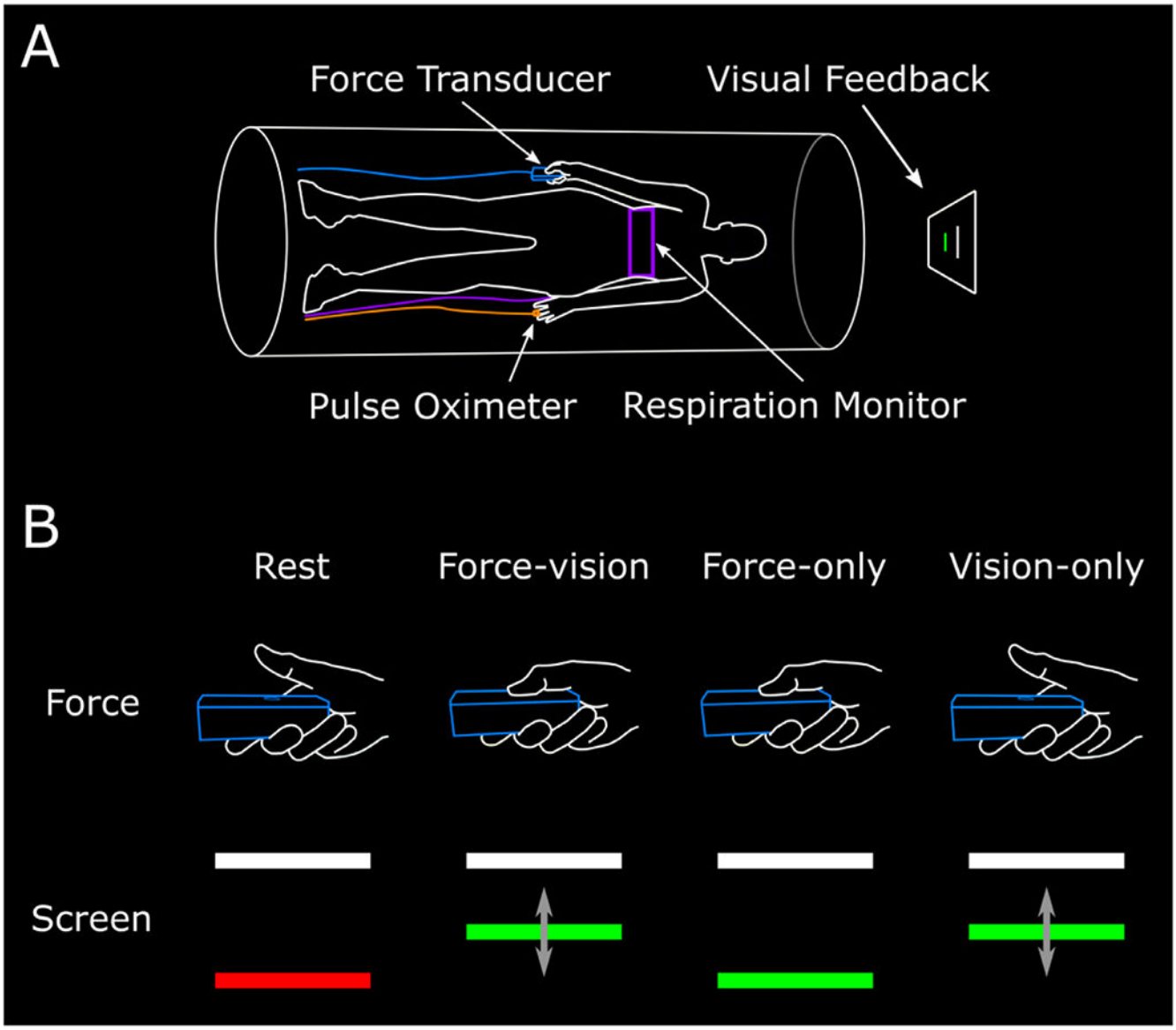

Fig. 1.

Task paradigm A) During the task fMRI scan, participants pressed on a force transducer with their right hand. As they pressed, a screen projecting to a mirror within the scanner gave visual feedback on the force they were producing. Throughout the scan, pulse and respiration signals were recorded using a pulse oximeter and respiration belt respectively. B) Participants performed 3 task conditions with periods of rest in between each task block. During the rest blocks, the bottom bar was red and participants did not produce a force (column 1). During the force-vision task condition, the bottom bar turned green and participants pressed on the force transducer. The bottom bar rose proportionately with the applied force and the goal was to make the bottom bar overlap with the top bar (column 2). During the force-only task condition, the bottom bar turned green, and participants pressed on the force transducer but the bottom bar did not move up; thus there was no visual feedback on the force produced (column 3). In this task condition, participants were

instructed to try to produce the same amount of force as in the force-vision condition. During the vision-only task condition, participants were shown a video of the visual stimulus from a previous trial but did not press on the force transducer (column 4).

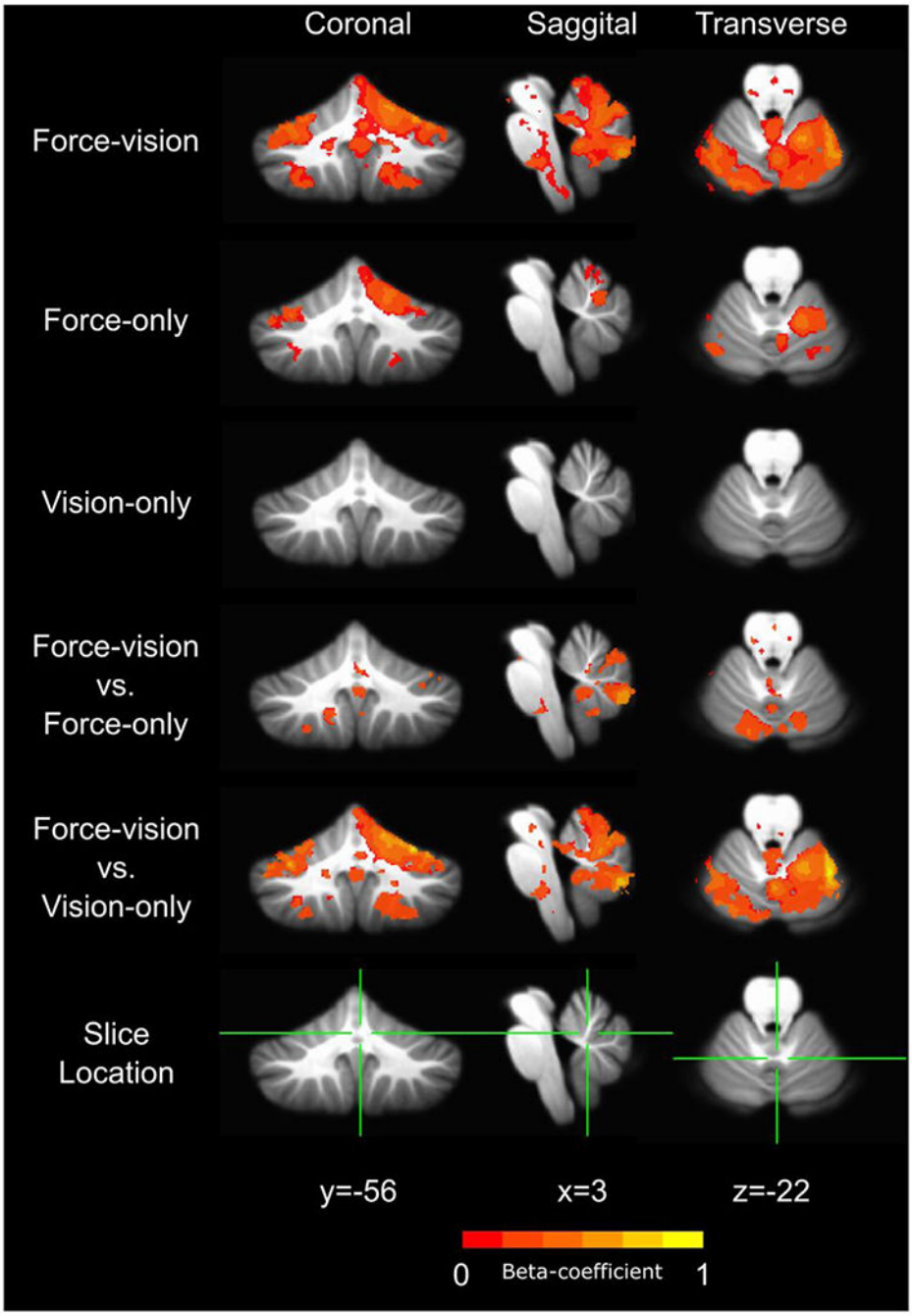

Fig. 2.

Task activation maps BOLD signal activity maps from the three task conditions are shown (rows 1–3). Green lines in the final row designate the locations of the displayed coronal, sagittal, and transverse plane slices.

Force-only and vision-only task conditions enable controlling for force-only and vision-only activity. Force-vision vs. force-only (row 4) and Force-vision vs. vision-only (row 5) contrast maps highlight regions of activity while controlling for force and vision activity

respectively. Brainstem visuomotor activity occurs in areas activated in both difference maps.

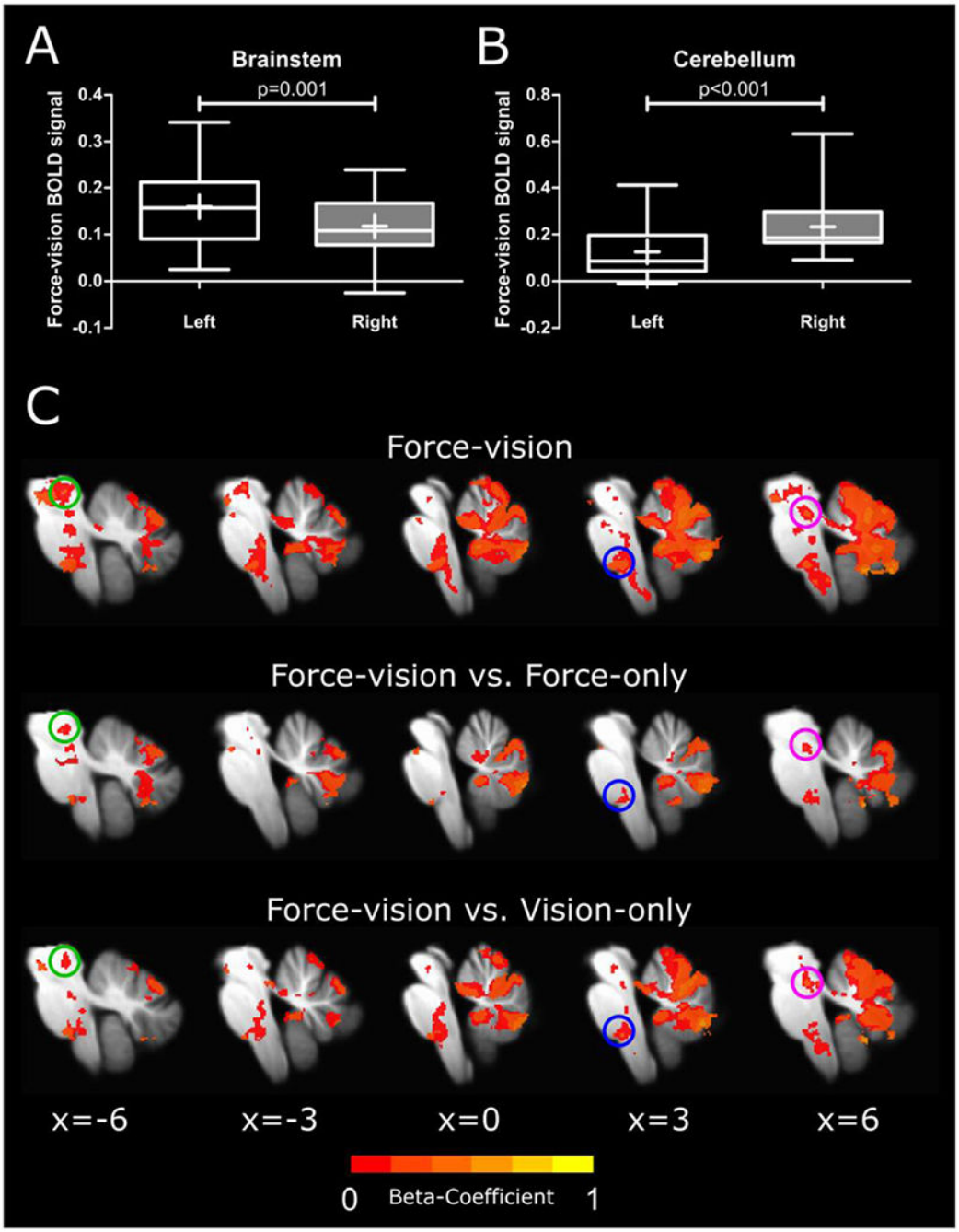

Fig. 3.

Force-vision activation patterns in the brainstem and cerebellum

Box plots comparing left (contralateral to the force-producing hand) and right (ipsilateral to the force-producing hand) brainstem (A) and cerebellum (B) force-vision activity. (C) Sagittal slices spanning the brainstem show the topography of the force-vision activity map, force-vision vs. force-only difference map, and force-vision vs. vision-only difference map. Green, blue and pink circles highlight three regions common to the force-vision activity and two difference maps. These regions best align with the region of the cuneiform nucleus,

basal pons, and region of the pedunculopontine nucleus. These regions are unique to the force-vision task condition and thus likely are regions involved in the integration of visual information for motor control.

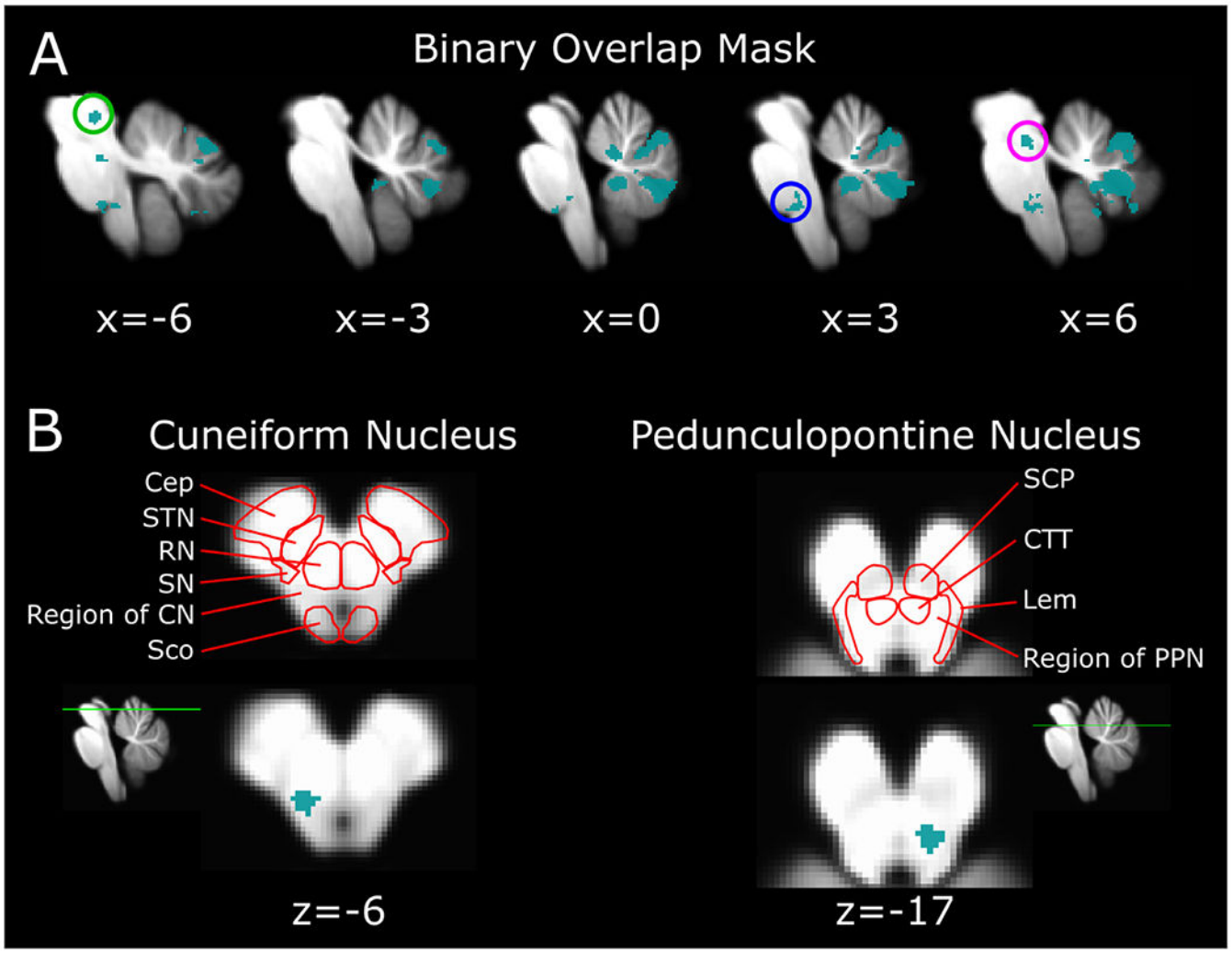

Fig. 4.

Visuomotor mask and midbrain localization

(A) A binary overlap mask was constructed to highlight regions common to the force-vision, force-vision vs. force-only difference map, and force-vision vs. vision-only difference map. Green, blue and pink circles highlight three regions common to the force-vision activity and two difference maps. These regions best align with the region of the cuneiform nucleus (CN), basal pons, and region of the pedunculopontine nucleus (PPN). (B) Horizontal plane slices of the CN and PPN activity clusters. Surrounding regions are outlined in red and were traced from an MNI atlas (Lucerna, 2002) and a paper outlining the PPN localization procedure used (Zrinzo et al., 2008). Cerebral peduncle (Cep), subthalamic nucleus (STN), red nucleus (RN), substantia nigra (SN), superior colliculus (Sco), superior cerebral peduncle (SCP), central tegmental tract (CTT), lemniscal system (Lem).

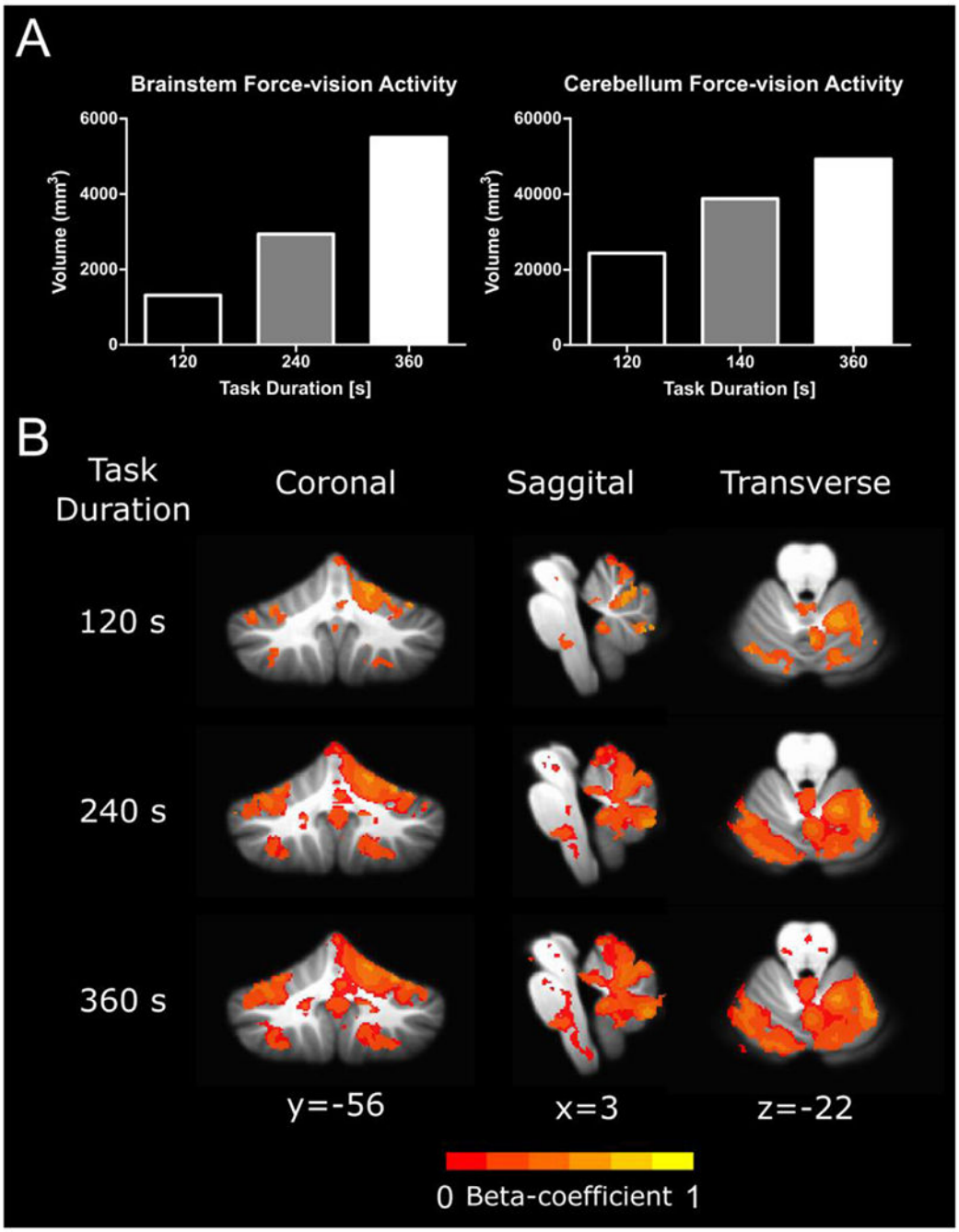

Fig. 5.

Brainstem and cerebellum activity as a function of task repetitions

A) The volume of force-vision activity in the brainstem and cerebellum are plotted against task repetitions.

B) Activity maps illustrate the detected force-vision activity in the brainstem and cerebellum that results from 120, 240, and 360 s of task duration which corresponds to 4, 8, and 12 repetitions of the 30 s task blocks.

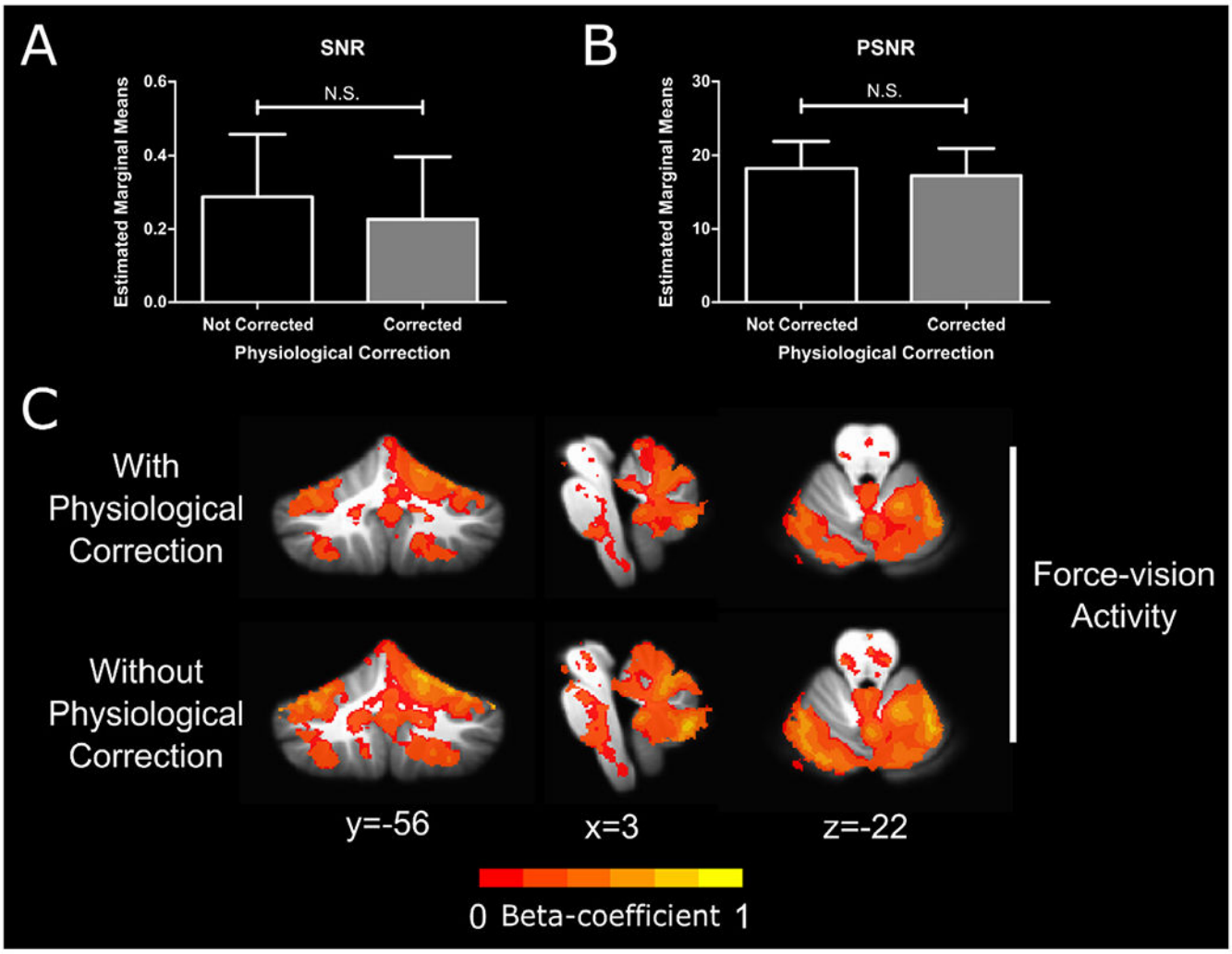

Fig. 6.

Effect of physiological correction on visuomotor signal

A and B) Estimated marginal means for the effect of physiological correction on the signal to noise ratio (SNR) and peak signal to noise ratio (PSNR) of each subject's beta-coefficient map are shown. Error bars designate one standard deviation. No significant effect (N.S.) was found in SNR and PSNR between with and without physiological correction. C) Force-vision activity maps with and without correction for physiological signals.

Table 1

Force-vision, force-only, and visuomotor activity clusters in the brainstem and cerebellum.

Region	Center of Mass (MNI)			Volume(mm^3)
	x	y	z	
Force vision				
Right Cerebellar Lobule IV, Lobule V, Lobule VI, Crus I, Lobule VIIb, Lobule Villa, Lobule IIIb, Lobule IX, Lobule X, & Dentate Left Cerebellar Lobule VI, Crus I, Crus II, Lobule VIIb, Lobule VIIIa, Lobule X, & Dentate Cerebellar Vermis VI-IX Caudal Pons & Medulla	2	−59	−32	52,352
Left Midbrain & Right Midbrain	−5	−23	−7	1559
Right Pedunculopontine Nucleus	8	−30	−17	315
Left Rostral Pons	−8	−30	−21	229
Anterior Rostral Pons	0	−21	−21	74
Force-only				
Right Cerebellar Lobule IV, Lobule V, & Lobule VI	17	−54	−20	5857
Left Cerebellar Lobule VI & Crus I	−33	−59	−28	1743
Right Cerebellar Lobule VIIb, Lobule VIIIa, & Lobule VIIIb	17	−62	−48	1259
Right Cerebellar Lobule VI	24	−67	−22	214
Left Cerebellar Lobule VIIb	−23	−69	−54	100
Left Cerebellar Lobule VIIIa	−31	−54	−47	90